Journal of The Electrochemical Society

A New Approach to Modeling Solid Oxide Cell Reactors with Multiple Stacks for Process System Simulation

Journal of The Electrochemical Society, 2022 **169** 054530

A New Approach to Modeling Solid Oxide Cell Reactors with Multiple Stacks for Process System Simulation

M. Tomberg,[1,z] M. P. Heddrich,[1] F. Sedeqi,[1] D. Ullmer,[1] S. A. Ansar,[1] and K. A. Friedrich[1,2]

[1]*German Aerospace Center (DLR), Institute for Engineering Thermodynamics, 70569 Stuttgart, Germany*
[2]*University of Stuttgart, Institute for Building Energetics, Thermotechnology and Energy Storage, 70569 Stuttgart, Germany*

Reactors with solid oxide cells (SOC) are highly efficient electrochemical energy converters, which can be used for electricity generation and production of chemical feedstocks. The technology is in an upscaling phase. Thereby demanding development of strategies for robust and efficient operation or large SOC reactors and plants. The present state of technology requires reactors with multiple stacks to achieve the appropriate power. This study aims to establish and apply a simulation framework to investigate process systems containing SOC reactors with multiple stacks. Focusing especially on the operating behavior of SOC reactors under transient conditions, by observing the performance of all cells in the reactor. For this purpose, a simulation model of the entire SOC reactor consisting of multiple stacks, pipes, manifolds, and thermal insulation was developed. After validation on stack and reactor level, the model was used to investigate the fundamental behavior of the SOC reactors and the individual stacks in various operation modes. Additionally, the influences of local degradation and reactor scaling on the performance were examined. The results show that detailed investigation of the reactors is necessary to ensure operability and to increase efficiency and robustness. Furthermore, the computing performance is sufficient to develop and validate system controls.
 [DOI: 10.1149/1945-7111/ac7009]

Manuscript submitted February 18, 2022; revised manuscript received April 8, 2022. Published May 26, 2022.

List of symbols

Latin Symbols

ASR	Area specific resistance
c	heat capacity
d	Differential operator
f	factor
H	Enthalpy
$\dot{H}$	Enthalpy flow rate
I	Electrical current
m	Mass
$\dot{m}$	Mass flow rate
n	number of control units
P	Power
p	Pressure
$\dot{Q}$	Heat flow rate
R	Resistance
RC	Reactant conversion
T	Temperature
t	Time
U	Voltage
x	Molar fraction

Greek Symbols

ρ	Density
Δ	Difference

Superscripts, Subscripts and Abbreviations

$'$	Inlet
$''$	Outlet
CU	Control unit
CV	Control volume
D	Dimension
DC	Direct current
EC	Electrolysis cell
el	Electrical
FC	Fuel cell
FC	Fuel flow channel
IC	Interconnects
id	Ideal
L/RTxSy	Left/Right Tower x, Stack y
max	Maximum
MEA	Membrane electrode assembly
min	Minimum
NiF	Nickel foam
OC	Oxygen flow channel
ohm	Ohmic
OP	Operation point
p	Constant pressure
PI	Proportional-integral
ref	Reference
SOC	Solid oxide cell
TN	Thermoneutral
WGS	Water-gas shift

Reactors with solid oxide cells (SOCs) are highly efficient electrochemical energy converters due to fast kinetics and low electrochemical losses.[1–4] They can be operated in fuel cell (SOFC) mode to convert chemical energy into electricity and in electrolysis (SOEC) mode for production of chemical feedstock.[5–7] Because of these features, they can play a central role in the energy system of the future. The SOC technology is gaining maturity and customers demand larger plants. Megawatt reactors are necessary, as current reactor sizes are small. This poses two main challenges: operation and upscaling of these reactors.

Contemporary large SOC reactors are set up by combining multiple SOC stacks, with common components such as manifolds or piping, into a large reactor module.[8,9] These components are arranged in a joint thermal envelope, so that the heat transfer takes place between the components and heat losses occur through the joint insulation.

Scientific research focuses on cells and single reactors often tested in furnaces. Experimental analysis of SOC reactors with multiple stacks is challenging as commercial reactors have limited sensors and critical operational characteristics are unknown. Therefore, system studies often assume SOC reactors to be assemblies of identically behaving cells and stacks. Experiments showed that this is not the case,[10–12] leading to an overestimation of

[z]E-mail: marius.tomberg@dlr.de

system performance and underestimation of potentially damaging operation.[13] Therefore, simulations to understand reactor behavior, to monitor and improve operation as well as robustness are advisable.

For example, Li et al.[14] described a reduction of system efficiency from 58% to 42% when a more detailed quasi-two-dimensional finite volume SOFC model was used for their system. Similar effects were also shown by Oryshchyn et al.[15] and Magistri et al,[16] who showed a reduction in the operating range. The models of Li et al.[14] and Oryshchyn et al.[15] are only suitable for steady-state simulation. However, it is also necessary to evaluate the operability in transient operation, e. g. to avoid damage due to temperature gradients. Several studies[5,17,18] on transient operation of cells and stacks were published. Due to the level of detail and the computation time required, these models are not suitable for system simulations. Others[16,19,20] are only suited for either SOFC or SOEC simulation. Therefore, Srikanth et al.[13] developed a detailed transient cell model for reversible SOC operation with a lumped, non-linear 1D resolution approach. Later, this model was extended to represent a full stack[21,22] and transferred to a simulation framework called TEMPEST.

This work presents an entirely novel transient simulation model of a complete SOC reactor, comprised of several single stacks, pipes, manifolds and insulation, which is fast and accurate enough for the following tasks. First, this approach supports designing and scaling electrochemical reactors. Second, the model enables the investigation of interactions between SOC reactor and the overall process system. Third, due to the transient character of this approach, reactor and system operation can be studied and operation strategies developed. Forth, the dependences between measurable parameters and non-measurable critical parameters can be investigated. After the modeling phase, the framework is used to examine operating points in both fuel cell and electrolysis modes. In addition, relevant issues such as the influence of local degradation and the scaling of the reactor are addressed.

The first part presents the general modeling approach for SOC reactors with multiple stacks in process systems. The modeling of individual components in the simulation framework, especially the stack, are described in the second part. Afterward it is shown, how this framework is applied to a commercial reactor including a validation. Finally, use cases of this model are presented.

Simulation Approach for SOC Reactors in Process Systems

SOC reactors with multiple stacks are modelled within the TEMPEST framework developed by the German Aerospace Center (DLR). TEMPEST is an object-oriented framework for transient simulations of process systems with electrochemical reactors. It can be easily applied to different cell architectures as electrolyte supported (ESC), electrode supported (ASC/CSC) or metal supported (MSC) SOCs. In addition, the framework can be used for modeling other technologies, such as alkaline electrolysis reactors. The focus is on operation and control strategies for SOC systems to increase efficiency and robustness. The framework is implemented in the equation-based object-oriented language Modelica using the commercial editor Dymola from Dassault systems.

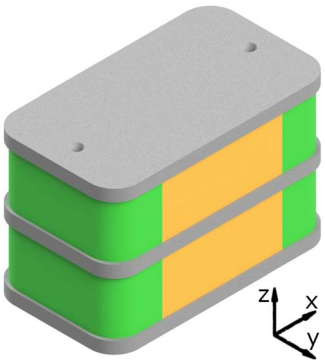

Figure 1. Stack model including active parts of the cells (orange), passive areas (green) as well as intermediate and end plates (grey). The *x*-axis is the gas flow direction. By considering these components, not only electrochemical effects but also the thermal effects of the end and intermediate plates as well as the passive area are taken into account.

The authors have shown before[10–12] that each stack in an SOC reactor operates in a different operating point due to heat losses, operating currents and uneven flow distribution of the gases. Implications like spatial and temporal temperature gradients inside these stacks need to be analyzed to ensure high performance and reliability. Therefore, in this work each individual stack in an SOC reactor is represented in the model. Furthermore, as heat and pressure losses result in temperature gradients and an uneven flow distribution, thermal insulation and internal piping need to be modeled. Considering all these points results in - complex models of SOC reactors with multiple stacks. Since the interactions between the SOC reactor and the surrounding system are also important for the development of robust and efficient operational strategies, the SOC reactor model must be applicable in system simulations. Therefore, a tradeoff between accuracy and speed of the simulation must be found.

For this purpose, an existing detailed stack model is simplified to allow its use in SOC reactor models with a high number of stacks. Subsequently, gas carrying and heat conducting components are modelled. Finally, the reactor models are assembled by arranging and connecting the component models.

Novel Modeling Concept and Implementation of SOC Reactors with Multiple Stacks

The full formulation of SOC reactors with multiple stacks consists of the simplified stacks, gas carrying and heat conducting components. Subsequently, the application of the framework to a specific commercial SOC reactor with 24 stacks and the validation of this model is presented.

Detailed SOC stack model.—The stack model is based on the 1D cell model developed by Srikanth et al,[13] which consists of subsections designated as a control unit (CU) in this work. The CU consists of 1D control volumes (CVs) with the length, dx, in the direction of flow. These CVs are the fuel flow channel (FC), the oxygen flow channel (OC), the membrane electrode assembly (MEA) and the interconnects (IC), which are connected perpendicular (Fig. 1: *z*-axis) to the flow in the configuration IC-FC-MEA-OC-IC. N number of CUs are then adjoined along the direction of flow to model the entire cell. This is illustrated in Fig. 1 of the referred publication by Srikanth et al.[13]

Mass balances are calculated for the fuel flow and oxygen flow channel, including the coupling of the two channels by the electrochemical mass flux. Both, fuel flow and oxygen flow channel, are modelled as well stirred reactors. Energy balances are calculated for all components of the CU, depicting the thermal coupling between them. Due to the operating temperatures and species considered, the steam methane reforming (SMR) and water-gas shift (WGS) reactions are assumed to occur in the fuel flow channel. The electrochemical reaction is assumed to occur at the electrode-electrolyte interfaces. Ohmic, activation and diffusion losses are modelled to calculated the cell voltages. The ohmic overpotential is calculated using the ohmic area specific resistance ASR_{ohm}, the current density i and a simple linear degradation factor, which can be used to simulate degraded stacks: $\Delta U_{\text{ohm}} = f_{ASR\ \text{ohm}} \cdot ASR_{\text{ohm}}(T)$. The activation overpotential is evaluated using the Butler-Volmer equation and the diffusion losses in the porous electrodes is calculated using the dusty gas model. The electrochemical parameters were determined by fitting the model to the activation and diffusion losses gained from experimental results by Riedel et al.[23,24]

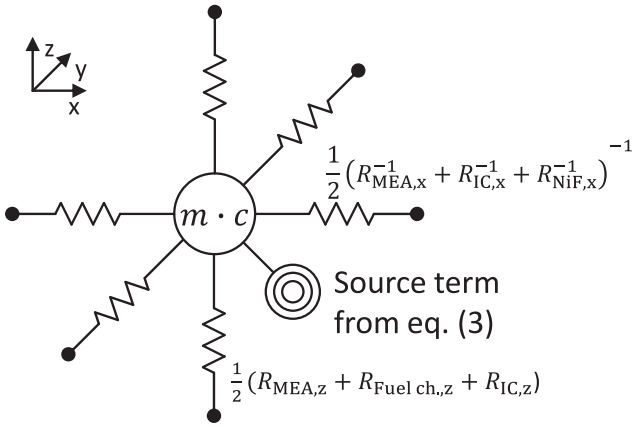

Figure 2. Equivalent thermal network of a simplified control unit. The resistors represent the lumped heat transfer per dimension, which is calculated based on the heat transfer phenomena in the individual layers (see examples in the figure).

Only the H_2-H_2O electrochemical reaction is considered, as the WGS reaction reaches equilibrium faster at the operating temperatures considered.[25,26] The ideal gas equation of state is used to close off the set of equations for the cell.

The stack model is assembled by adjoining the CUs vertically, resulting in a 1D + 1D stack model. Heat transfer to the surroundings, such as radiation and conduction, is modelled using the thermal properties of the materials and gases. End plates and Intermediate plates, used for thermal distribution and mechanical stability, are also included and modelled in a similar way to the IC. The end plates are connected to the first and last cells, while the intermediate plates are placed between some cells. Furthermore, the passive area of the stack that encloses the electrochemically active cell part is modeled. It has essentially the same structure as the active area. However, electrodes and foam in the fuel channel are missing so that no reaction is taking place. Due to the heat conduction in the solid material against the flow direction of air and fuel, there is a preheating of these gases, which is considered. The passive area is divided vertically into two parts. The part next to the active part of the stacks consists of CU, whose design is similar to the cells' CU. However, as no chemical or electrochemical reactions are taking place, their terms disappear from the equations. The part next to the oxygen side compartments does not consist of the horizontal fuel flow cannels but vertical fuel manifolds. These are modelled using a lumped approach for the bottom half and top half of the stack, which considers the convective heat transfer and the pressure loss in the vertical pipes. Between the bottom and top half, a flow split takes place depending on the downstream pressure losses. In a second step this flow is divided to the single cells. Figure 1 shows all the components of the stack model.

A larger number of such detailly modeled stacks is not applicable in system simulations. For large multi-reactors consisting of several sub-reactors with hundreds of cells, this results in a large computational effort. Therefore, some detailed CUs will be replaced by a number of simplified CUs. The thermal properties of both types of CUs will be considered. The simplified CUs assumptions are presented below.

Simplification of SOC stack model for usage in reactors with multiple stacks.—Contrary to the detailed control units,[13] in the simplified control units, the mass and thermal capacity of the electrodes and the electrolyte (MEA) as well as the interconnect (IC) and if present nickel foam (NiF) are lumped.

$$m_{\mathrm{Simp}} = m_{\mathrm{MEA}} + m_{\mathrm{IC}} + m_{\mathrm{NiF}} \quad [1]$$

$$c_{\mathrm{Simp}} = m_{\mathrm{Simp}}^{-1}\left(m_{\mathrm{MEA}}\, c_{\mathrm{MEA}} + m_{\mathrm{IC}}\, c_{\mathrm{IC}} + m_{\mathrm{NiF}}\, c_{\mathrm{NiF}}\right) \quad [2]$$

Equation 3 is the energy balance of the simplified control units. The storage term can be found on the left side of the equation. The heat transfer over the boundaries of the control unit is described by the term $\sum \dot{Q}_i$. The terms $\Delta\dot{H}_{\mathrm{OC}}$ and $\Delta\dot{H}_{\mathrm{FC}}$ describe the change in the enthalpy flows in the oxygen and the fuel channel of one control unit including the enthalpy of formation (see Eq. 4). The single enthalpy flows are calculated based on the value of the next detailed control unit called the reference (ref) control unit. To account for the difference in temperature between the simplified and its reference control unit, the value is corrected using the heat capacity (Eq. 5). In contrast to the detailed CUs, a precise calculation of the overpotentials is not performed. The electrical power of one control unit is calculated (Eq. 6) using two assumptions. First, the ideal voltage of the simplified and the reference control unit are equal. Second, the overpotential of the simplified control unit can be approximated by multiplying the overpotential of the reference CU with the ratio of the temperature dependent ohmic area specific resistance ASR_{ohm} to perform a temperature correction. The ohmic ASR relation taken from Riedel et al.[23] was determined using experiments on stacks, which were composed of cells with the same design and materials. The ideal voltage of the simplified control units is not temperature corrected, as the temperature dependency is around 36 times smaller compared to the ohmic ASR's dependency.[23]

$$\frac{d\left(m_{\mathrm{Simp}}\, c_{\mathrm{Simp}}\, T\right)}{dt} = \sum \dot{Q}_i + \underbrace{\Delta\dot{H}_{\mathrm{OC}} + \Delta\dot{H}_{\mathrm{FC}} + P_{\mathrm{el}}}_{\text{Figure 2: Source term}} \quad [3]$$

$$\Delta\dot{H}_i = \dot{H}''_i - \dot{H}'_i \quad [4]$$

$$\dot{H}'_i = \dot{H}_i^{\mathrm{ref}'} + \dot{m}'_i\, c_{p,i}^{\mathrm{ref}\,'}\left(T'_i - T_i^{\mathrm{ref}\,'}\right) \quad [5]$$

$$P_{\mathrm{el}} = -\left(U_{\mathrm{id}}^{\mathrm{ref}} - \left(U_{\mathrm{id}}^{\mathrm{ref}} - U^{\mathrm{ref}}\right)\frac{ASR_{\mathrm{ohm}}(T)}{ASR_{\mathrm{ohm}}(\mathrm{T}^{\mathrm{ref}})}\right)\cdot I^{\mathrm{ref}} \quad [6]$$

Figure 2 shows the equivalent thermal network inside a simplified control unit consisting of the lumped heat capacity and thermal resistors. The source/sink in the equivalent thermal network represents the electrochemical losses and the change in the enthalpy flow of the reference cell (see Eq. 3).

The heat transfer in flow direction is lumped into a single heat conduction element, which accounts for the heat flow through the interconnect, the foam in the fuel channel, the electrodes and the electrolyte. The heat transfer along the *y*-axis (rf. Fig. 1) was not changed compared to the detailed cells. Since within the simplified cells, gas volume flows and electric current are not calculated, the temperature of the outlet volume flows and the total stack voltage must be calculated. The temperature of the outlet flows is based on the temperature of the detailed cells and the outlet temperature profile of detailed and simplified cells in the *z*-axis. The stack voltage is the sum of the cell voltages. In case of the simplified cells, the average simplified control unit voltage (derived from Eq. 6) is used.

To further decrease the complexity and the calculation effort, several simplified control units can be merged in z-direction. In this case, an assembly of control unit cells is assumed to behave equally. This results in the following energy balance with the vertical block size number n_{vert}.

$$n_{\mathrm{vert}}\frac{d\left(m_{\mathrm{Simp}}\, c_{\mathrm{Simp}} T\right)}{dt} = \sum \dot{Q}_i + n_{\mathrm{vert}}\Delta\dot{H}_{\mathrm{OC}} + n_{\mathrm{vert}}\Delta\dot{H}_{\mathrm{FC}} + n_{\mathrm{vert}}P_{\mathrm{el}} \quad [7]$$

Gas-carrying model components.—The reactant gases must be supplied to the cells in SOC reactors. In principle, two designs are

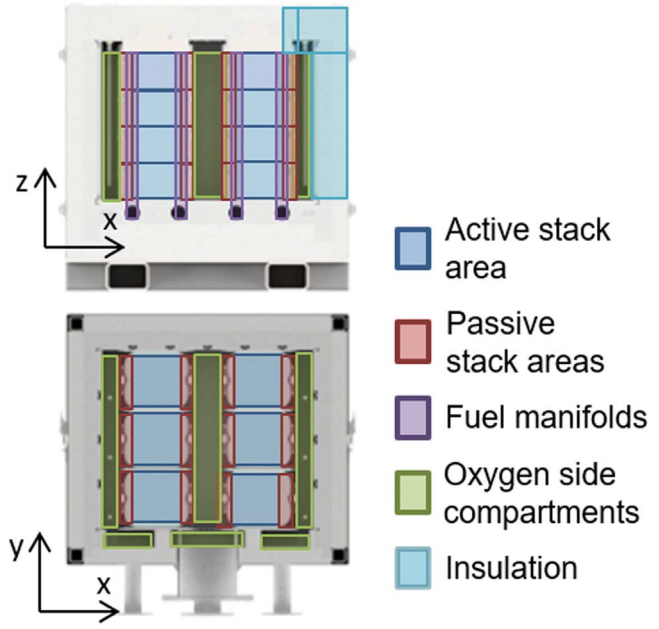

Figure 3. Front and side of the SOC reactor including all relevant components. The overlay for the insulation depicts three exemplary insulation blocks.

distinguished. First, the distribution of the gases can take place within the stack. For example, the gas can enter the bottom of the stack and be vertically routed to the top. Second, the division of the gases takes place outside the stack. This case would be an open electrode design. For example, the entire stack or even a cluster of stacks is surrounded by an enclosure containing the gas, which is then distributed to the cells. For example, the F10 stack from Forschungszentrum Jülich has internal manifolds for both electrodes.[27] Other manufacturers like Sunfire use a stack-internal manifold for the fuel electrode, and an open design for the oxygen electrode. Both variants can be modeled in the framework. In the following, the latter combination is considered as described above for the detailed SOC stack model.

In case of gas compartments, for which the throughflow is not trivial (e.g. volumes in front of or after the stacks), these volumes are considered to be zero-dimensional. However, the heat transfer is modelled separately for each area that is surrounding the volume. Convection between surfaces and gases as well as radiation between surfaces are modelled with standard approaches according to geometry.

For standard components, such as valves, flow mixers, and pipes, the modelica library ThermoPower by Casella et al.[28,29] is used. Some components such as pipes are designed as 1D models. The library models use mass, energy, and momentum balances. Furthermore, well-established empirical correlations are used where necessary. For further information on these components, see the referred documentation.[28,29]

Heat-conducting model components.—Heat capacity and heat conductivity were modelled based on the used materials. Where necessary, temperature dependent correlations were used. For example, the microporous insulation material SILCAPOR Ultra 950 varies from 0.022 W (m K)$^{-1}$ at 200 °C to 0.044 W (m K)$^{-1}$ at 800 °C.[30] In the case of plates, it is necessary to check whether they can be considered as thin. In this case heat conduction through the plate's thickness can be assumed as infinite, while perpendicular directions can be assumed zero.

Results and Discussion: Validation and Analysis

The described modeling framework is applied to a commercial SOC reactor with 24 stacks from the company Sunfire. Validation and operating analysis are performed both for the SOC reactor as well as in detail for one stack.

Design and parameterization.—An example of a large SOC reactor that can be modeled with the framework is Sunfire's Stack Unit.[31] It consists of six towers with four stacks with 30 cells each. The stacks have an open oxygen side manifold and consist of electrolyte supported cells, each with an active area of 127.8 cm^2. Further details on the used materials and layer thicknesses can be found in Riedel et al.[23] and regarding the model parameterization in Srikanth et al.[13]

Figure 3 shows the front and side view of the SOC reactor. The oxygen side flow enters its compartment between the two rows of towers. After flowing through each reactor, the oxygen flow is collected in an outlet compartment and exits the reactor through the two outlet flanges. The fuel gas flows into the bottom of the reactor and is distributed to the individual stack towers via two horizontal pipes. The outlet piping is equivalent to the inlet. Due to the open oxygen electrode design, the stacks and oxygen side compartments are enclosed in a single metal hood. The thermal insulation is located outside this metal hood. Thin layers of electrical insulators are located between the stack towers. The stacks are labelled according to their location in relation to the inlet and outlet flanges and the base plate, respectively. The tower rows are designated as left (L) or right (R). The towers (T1–3) and the individual stacks in the towers are numbered consecutively (S1–4). Neighboring towers (e. g. LT1 and LR1) are electrically connected in series resulting in three independent power channels. All geometries and dimensions were taken from manufacturer's specifications and drawings. The material properties, for example of the insulation, were obtained from the suppliers' data sheets.

For research purposes the SOC reactor was specially equipped with numerous sensors that are not placed in the commercial product. Each stack is equipped with a thermocouple that measures the temperature in the oxygen flow channel at the outlet of the center cell of each stack. In addition, two stacks have four additional thermocouples at 0%, 25%, 50% and 75% of the cell length (similar to the configuration in Fig. 5). The voltage of each stack is measured via voltage taps at the endplates. Thus, stack voltages were measured and cell averages calculated.

For all simulations the following boundary conditions were applied. The downstream pressure was set to 101325 Pa and the ambient temperature T_{amb} to 20 °C. During the validation experiments the boundary temperature at the SOC reactor's front face (xy-plane) differs from T_{amb} and is set to 700 °C. This was done, because the test rig has an insulation box on this face that contains the hot gas components. The inlet temperatures were applied to the inlet flanges (Fig. 3). Unless otherwise noted, the SOC reactor was parameterized consisting of 24 stacks with 30 cells each. Each stack has 8 CUs in x-direction and 13 in z-direction with vertical block sizes of 4, 3, 3, 2, 2, 1, *, 1, 2, 2, 3, 3, 4. The passive areas have 2 CUs in x-direction and an identical configuration in z-direction.

Validation on SOC reactor level.—For validation the SOC reactor was experimentally tested on the DLR test rig GALACTICA, which was designed for the characterization of SOC reactors with multiple stacks. Details can be found in Ref. 32. A detailed experimental analysis of the operating points used for the validation and further operation details will be given in another publication. The validation is divided into two steps. In the first step, temperatures and voltages of all individual stacks were compared. The temperatures are measured at the outlet of each stack. The voltages measured at the endplates of each stack and divided by the number of cells. In the second step, the temperature profile in a selected stack was examined during stationary operation.

The transient validation (see Fig. 4) was performed in water electrolysis mode with an inlet composition of 90% H_2O and 10% H_2 on the fuel side and air and the oxygen side. The inlet temperatures of fuel and air were set to 810 °C. While the air flow

was kept constant at 42.9 g s^{-1} (per cell: 0.06 gs^{-1} = 2.8 slpm), the fuel flow was calculated to result in a reactant conversion of 70%. The fuel flow was always changed before the current, resulting in a short period of a lower conversion starting at t = 150 min. The experimental values are shown in two ways. Firstly, the minimum and maximum of all values are shown. Secondly, before calculating minimum and maximum values, the values are averaged along the axis of symmetry (e.g. T2S1 = 0.5 (LT2S1 + RT2S1)). This is done to reduce random effects like manufacturing tolerances.

For the stationary points at 0, 150, and 300 min the simulated temperatures at the thermocouple locations are always between the minimum and maximum measured temperatures with a maximum offset of 8.5 K. A similar behavior can be observed for the voltages with a maximum offset of 30 mV. Simulated temperatures and voltages follow the experiments very well during the transients. This can be seen for changes in both, electrical current and reactant conversion. In the simulation results of a second transient, a similar behavior can be observed. When the fuel flow is increased, temperatures and voltages drop due to the low reactant conversion. The increasing electrical current leads to a higher temperature and an increased voltage.

In general, the qualitative results match well. For example, during the current ramp at t = 150 min, the minimum and maximum temperature values converge in the simulations and the experiments. However, in the simulation the minimum and maximum temperature values converge also with increasing current. In standby the difference is around 9 K in simulation and experiments. While the difference increases slightly in the experiments, it decreases in the simulation to 5 K at 0.52 A cm^{-2}. This can be explained by the different performances of the individual stacks. In standby, at 0 A, the minimum and maximum temperatures and thus the difference match. The differences in the temperatures result from heat losses and pressure losses, which can be assumed to be modelled very accurately. With increasing currents, the electrochemical losses start to play an important role in the energy balance of the individual stacks. As the electrochemical parameters in the simulation are the same for all stacks, the differences between minimum and maximum temperatures decreases. In reality, the electrochemical performances of the stacks vary due to manufacturing tolerances and uneven degradation. To investigate this further, the temperature values were averaged along the axis of symmetry. This leads to a reduction of differences between minimum and maximum, which is slightly decreasing with increasing current. This supports the argument that the deviations can be explained by random effects as tolerances and uneven degradation. In order to be able to discard errors in the stack model or the electrochemical equations, the stack model itself is validated subsequently. Furthermore, the influence of degraded stacks is investigated eventual.

Three operating points (see Table I) were selected to validate the axial temperature profile in one individual stack, which was equipped with additional thermocouples for this validation. First, water electrolysis operation at an electrical current of −0.39 A cm^{-2} was investigated. At the second operating point, the electric current was increased to −0.52 A cm^{-2}, and at the third operating point, the gas composition was changed so that a co-electrolysis operation was performed.

Figure 5 shows the simulated temperature profiles in the flow direction of the center cells of stack LT2S3. The profiles show the endothermal characteristic of the first and third operation point as well as the nearly isothermal behavior of the second. At this point, it should be noted that isothermal operating points have a curved temperature profile due to heat losses. In an adiabatic system, an isothermal and a thermoneutral (with $U = U_{TN}(T_{inlet})$) operating point would match. Operation point three was even colder than operation point two, which, in principle, can be due to the reverse water-gas shift reaction taking place, a change in the heat capacity flow of the fuel gas or the smaller air flow. The heat capacity flow can be ruled out as the OP3 (4.40 W K^{-1}) $ha^{-1}s^{-1}$ an even higher heat capacity flow than OP1 (4.07 W K^{-1}). The red line shows the simulation results for OP3 using the air flow from OP1. It shows that the lower air mass flow has an influence but the reverse water-gas shift reaction dominates. This can also be seen from the different slopes in OP1 and OP3.

The agreement of simulation results and experimental results is sufficiently accurate to use the model to develop operating strategies and control approaches. This will be presented below. Furthermore, it was shown that with the simulation, it is possible to separate individual effects and thus explain the measured data.

Validation on stack model level.—The stack is the component that is the most challenging to model and has the largest impact (rf. reactor validation). The simplified stack model as well as the

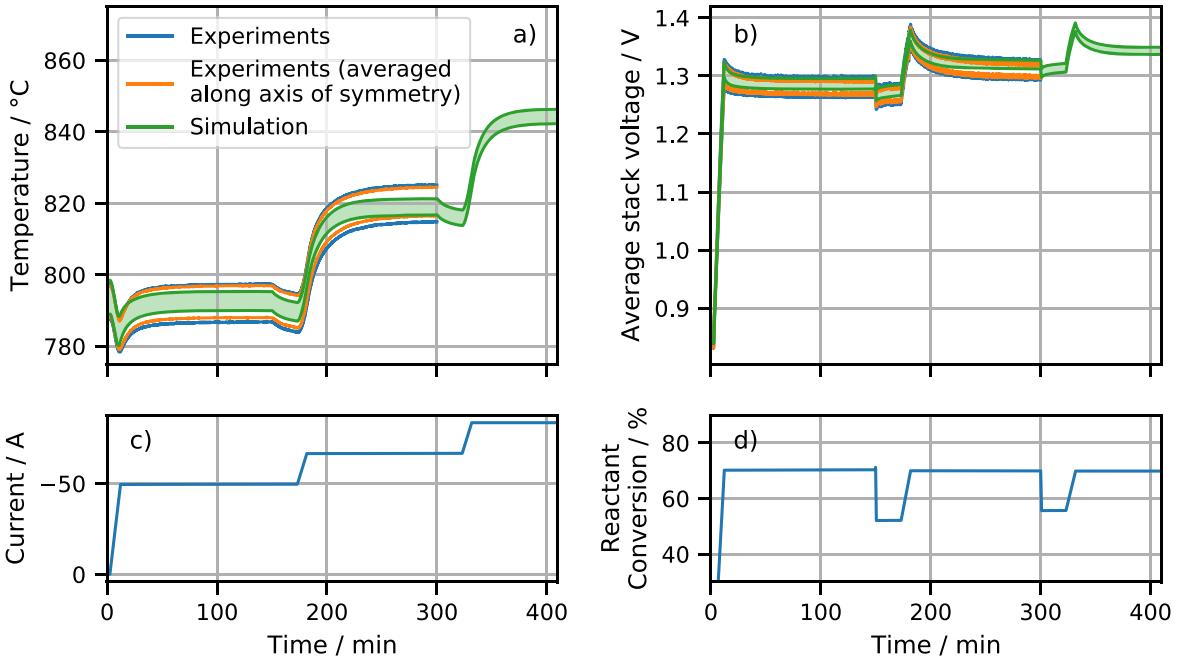

Figure 4. Validation and extrapolation of the SOC reactor model in water electrolysis mode. In the temperature (a) and voltage (b) plot all measurable values between the minimum and maximum are shown as an area. Furthermore, electrical current (c) and reactant conversion (d) are shown.

Table I. The selected operating points for validation of the temperature profile in flow direction.

Opera-tion point	Current density i	Inlet gas molar fractions				Air flow $\dot{m}_{air}$	Inlet temperatures		Average cell voltage U
		x_{H_2}	x_{CO_2}	x_{CO}	x_{H_2O}		$T_{Gas,in}$	$T_{Air,in}$	
1	−0.39 A cm^{-2}	0.10			0.90	42.9 g s^{-1}	813.2 °C	810.8 °C	1.279 V
2	−0.52 A cm^{-2}	0.10			0.90	28.8 g s^{-1}	810.4 °C	811.0 °C	1.311 V
3	−0.39 A cm^{-2}	0.07	0.31	0.03	0.59	21.4 g s^{-1}	809.2 °C	808.6 °C	1.344 V

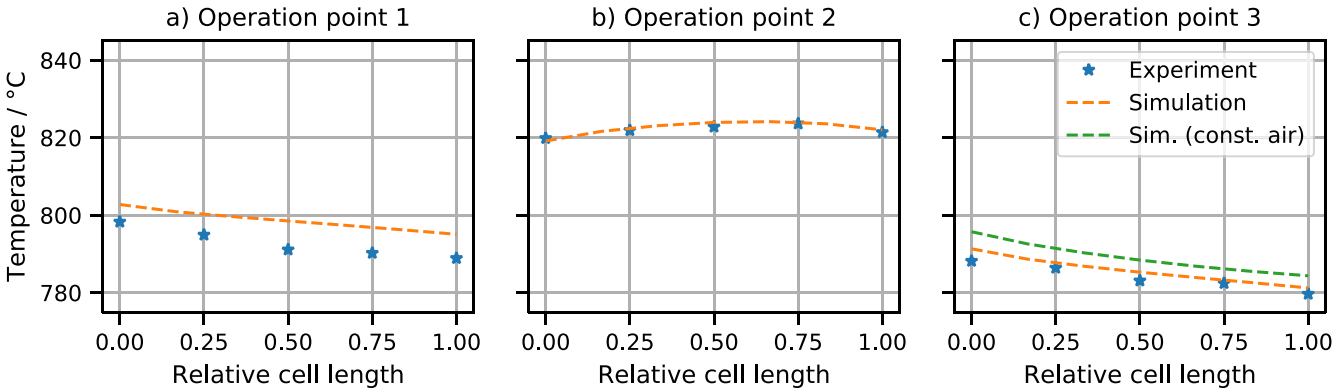

Figure 5. Validation of the SOC reactor model by comparison of temperature profiles in flow direction for the three operation points listed in Table I.

sensitivity of the novel modeling approach are investigated and discussed below, since the accuracy and computation time of the SOC reactor model strongly depend on the stack model due to error propagation and exponential computation time growth, with an increasing number of stacks.

The validation experiments were performed on a test rig located at the stack's manufacturer Sunfire. The test rig's insulation is similar to the reactor module. Therefore, the effects of heat losses were considered in the validation. Unfortunately, the test rig had an air leakage in front of the stack inlet. Therefore, instead of the air mass flow set in the experiment, a temperature controller was used to determine the air mass flow. An analogous temperature controller was set up within the model to match the experiments. In the simulations the center cell of each stack is calculated with detailed CUs, while all other cells are simplified.

Qualitative results.—Figure 6 shows the 2D representation of the temperature profile along the x- and z-direction in fuel cell and electrolysis mode. As was to be expected, the local temperature gradients were smaller in electrolysis mode. For the qualitative and detailed validation of the model, the fuel cell operation was chosen, as errors will be more pronounced due to the higher gradients.

In both cases, the hotspots were located at approximately 3/4 of the cell length. In fuel cell mode, the temperature gradients were higher both horizontally and vertically. The higher thermal conductivity of the intermediate plates between cells 10 and 11 as well as cells 20 and 21 was clearly evident and leads to an equalization of the horizontal temperature profile at these cells. The positions of the thermocouples used for validation below are each marked with an "X".

Quantitative results.—Within the validation, five experimental operating points were used. The stack was operated with a molar mixture of 40% hydrogen and 60% nitrogen at a reactant conversion of 70%. The fuel gas inlet temperature was 750 °C, while the air inlet temperature and electric current were varied (see Table II). By adapting the air mass flow, the temperature at ¾ of the cell length of cell 15 was set to 860 °C. Eight thermocouples were available for validation; as well as a voltage tap every three cells, resulting in 10 voltage measurements. The position of the thermocouples is indicated in Fig. 6.

Figure 7 shows the comparison of simulations and experiments. The first row shows the horizontal temperature profile for the center cell; the second row, the vertical temperature profile in the middle of the stacks; and the third row, the voltage. For the experimental data, the measured voltages and the average voltage are shown. In the case of simulation results, the voltage of the detailed cell and the calculated average voltage are shown.

In the diagram, two sets of parameters are considered. First, the "base," which has eight control units along the x-axis and vertical block sizes of 4, 3, 3, 2, 2, 1, *, 1, 2, 2, 3, 3, and 4, resulting in a higher accuracy near the detailed cells, marked here with an asterisk. Second, the "detailed" case, has a no vertical lumping and 16 control units along the x-axis. Good agreement between experiment and simulation can be shown for all operating points. As expected, the "detailed" case results in better agreement between simulation and experimental data, especially in terms of temperatures. However, agreement between the experimental data and the "base" case simulation remain reasonably accurate. For the upper and lower cells, the effect of the vertically lumped cells is evident.

Both sets of parameters, "base" and "detailed" show good agreement between simulation and experimental data. The strength of the simplification approach becomes clear when the computation times for all operating points and the transients in between are compared. The computation time of the calculation with the "detailed" parameter set was 134 s. In comparison, the computation time for the "base" case was reduced by a factor of 9 to 15.2 s. These as well as the following results were obtained on a workstation with an Intel® Xeon® W-2235 CPU.

Sensitivity analysis of simplification parameters.—Since the accuracy and the computation time have a high influence on the SOC reactor simulation due to error propagation and exponential computation time growth, the effect of the number of control units along the x-axis and the vertical block size is examined below. For clarity, a representative operating point was chosen for each parameter.

To determine the influence of the number of control units along the x-axis$n$, multiples of four were chosen to harmonize control units and thermocouples. Figure 8 shows that only 4 control units lead to an unsatisfactory result. The difference between 12 and 20 control

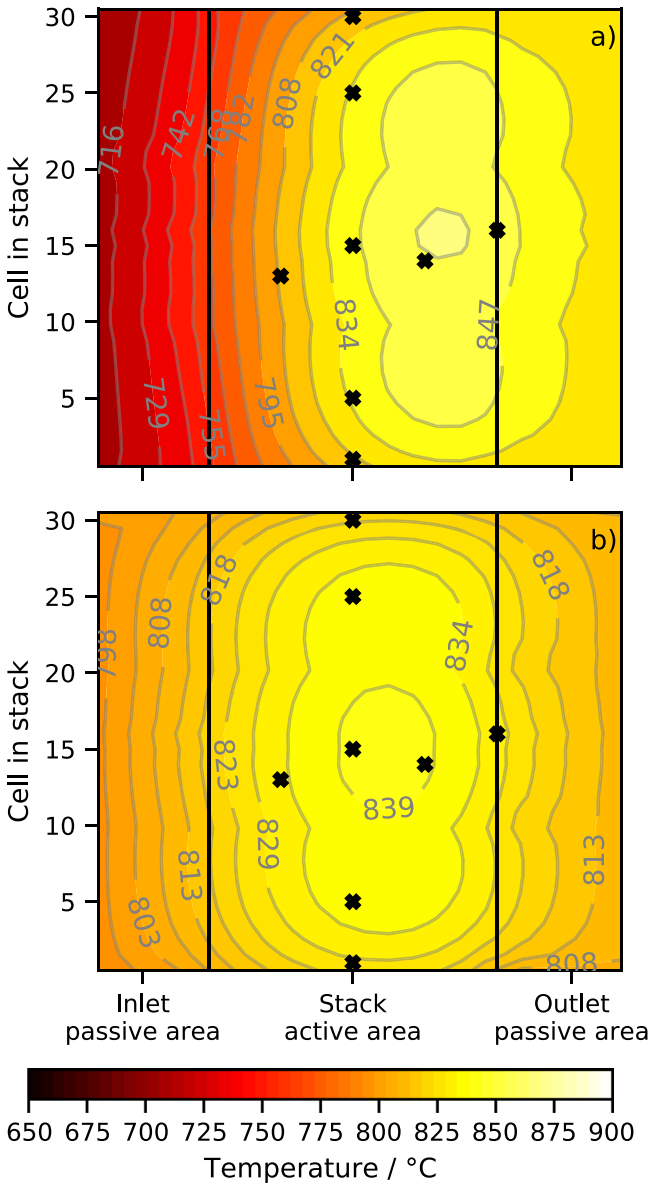

Figure 6. 2D representation of the temperatures in the xz-plane at y = 0. The hotspot of the cells is around 70% of cell length. The influence of the intermediate plates is clearly visible around cells 10 and 20. (a): Fuel cell operation (40% H2, 60% N2, 600 °C inlet, 0.28 A cm^{-2}), (b): Electrolysis cell operation (95% H2O, 5% H2, 820 °C inlet, 40% O2 outlet, −0.63 A cm^{-2}). All positions of the thermocouples are marked with a "X".

Table II. Electric current and air inlet temperature of the fuel cell operation points used for validation.

OP	1	2	3	4	5
Current density/A	0.23	0.31	0.28	0.28	0.23
Air inlet temperature/°C	650	600	600	650	600

units was small. With 8 control units the results were slightly worse with an increased temperature difference at the inlet. The voltage deviation decreased with an increasing number of control units. The calculation time increased with about $t_{calc} = 4\exp(0.17n)$. Depending on the application, 8 or 12 control units should be used.

In the next step, the impact of the size and number of the vertical lumped blocks was investigated (Fig. 9). The variation of the vertical merging had almost no influence on the horizontal temperature profile. As expected, on the other hand, the vertical profile was strongly influenced. The calculation of the average voltage lead to good results, except in the most simplified case. The base case gave very good results and showed a high numerical stability.

In summary, the base case simulation parameterization, which was also used for SOC reactor results, gives reasonable accuracy at high computational speed, and will continue to be used in this work.

Results and Discussion: Application of the Model

Investigation of operating points, fuel side gases and operating modes.—A major advantage of SOC reactors is their flexibility due to their capability of reversible operation and fuel or product gas flexibility. The entire operating range of such reactors can be mapped and investigated with the simulation framework. Figure 11 shows operation at eight operating points, including transitions from SOFC operation with internal methane reforming, to co-electrolysis operation. No real SOC system, perhaps with the exception of a reversible SOC system, would operate over such an extremely wide operating range. However, this simulation offers the possibility to directly compare the different operating points with similar boundary conditions.

In contrast to the validation experiments, for these transient simulation results, several controllers were used. The fuel flow was controlled by an open loop controller that kept the reaction conversion at 75%. On the oxygen side, air was used. Air mass flow, as well as air and fuel inlet temperatures, were set by a temperature controller (Fig. 10) designed to operate at all non-isothermal operation points. It consists of a PI controller and a calculation block. The PI controller outputs a signal between 0 and 1. 0 means maximum cooling; 1 maximum heating. The calculation block uses this signal to determine the air and fuel gas temperature via a linear correlation, and the air mass flow with a quadratic function. The minimum and maximum inlet temperatures and air mass flow, are specified based on the reactor's limits. A quadratic function is used to keep the air mass flow low at operating points that require only low cooling or heating power. This reduces the required air fan power and may reduce the air preheater power. The maximum air flow $\dot{m}_{air}^{max}$ is set to 100 g s^{-1}, the minimum $\dot{m}_{air}^{min}$ to 12 g s^{-1}, the maximum fuel and air inlet temperature T_i^{max} to 850 °C, and the minimum T_i^{min} to 650 °C. During isothermal operation, the controller is bypassed and the air mass flow and the inlet temperatures are set to $\dot{m}_{air}^{min}$ and 830 °C, respectively.

Figure 11 shows the time dependent behavior of current density, temperatures, their local difference, and gradient; as well as the behavior of the temperature controller, in the different operational modes. It demonstrates that, the SOC reactor model can be used for all SOC operating modes and a wide range of gas compositions. Subplot (a) shows the set current density, the average stack voltage, and the output signal of the temperature PI controller. Subplot (b) shows the simulated temperature distribution at the thermocouples, as also shown in the validation, compared to the temperature distribution of the entire reactor. Subplot (c) shows the spatial temperature difference across the cells. The last subplot (d) shows the temporal temperature gradients in the reactor.

The operation starts in fuel cell mode using pure methane as fuel. Despite the high current density, only moderate cooling is required due to the internal reformation. The switch to pre-reformed methane (steam to carbon ratio: 2) is smooth. Cooling needs to be increased and the difference between minimum and maximum temperature (second plot) increases even more. Operation with hydrogen is similar. Subsequently the operation switches from fuel cell to an endothermic steam electrolysis point. This leads to larger temperature gradients and the temperature controller switches to heating (value > 0.5). Afterwards the controller is bypassed to allow isothermal operation leading to very small spatial temperature differences. In the exothermic electrolysis points moderate cooling

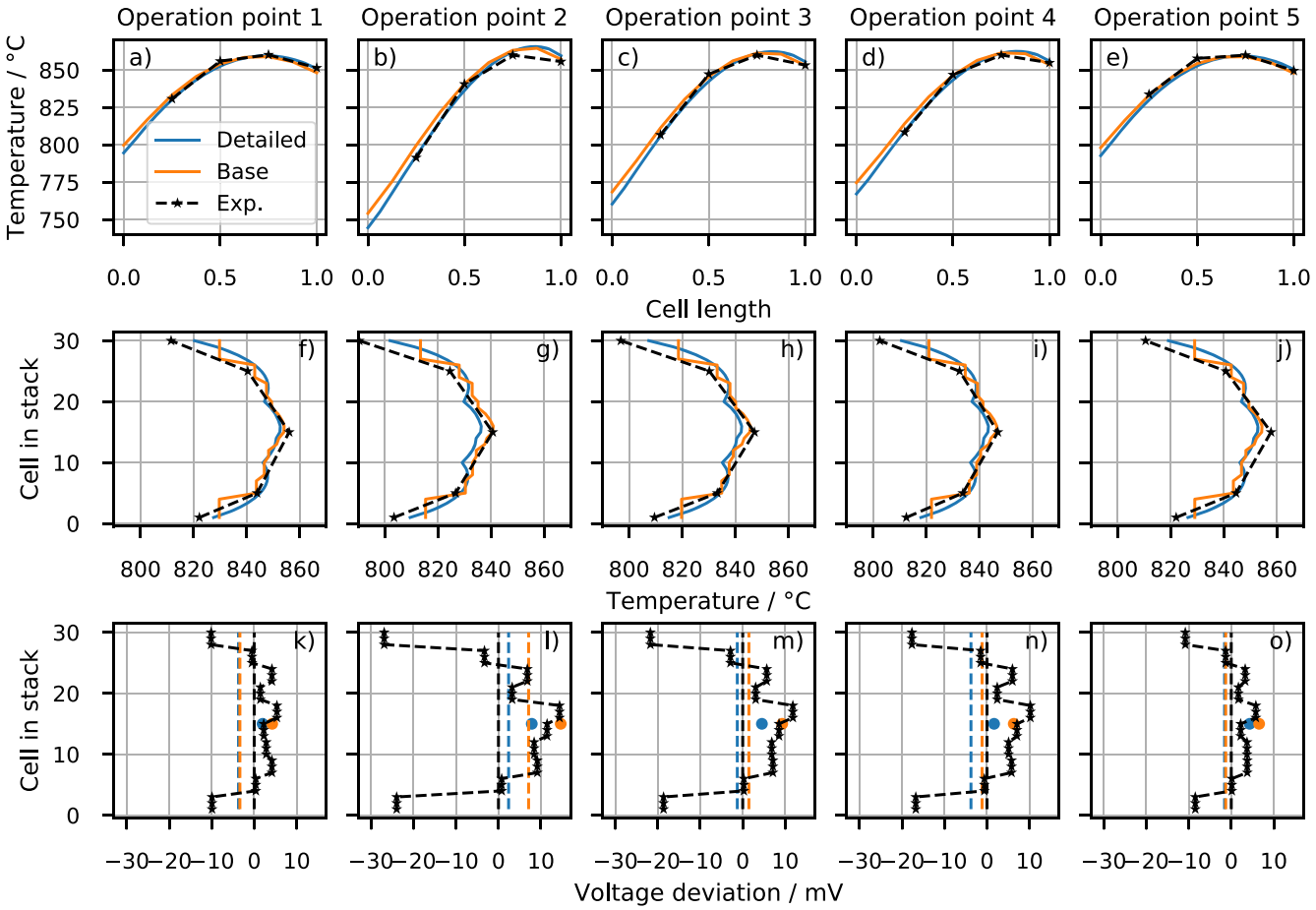

Figure 7. Validation of the simplified stack model. The voltage plots ((k)-(o)) show the experimental voltages (blocks of three cells), the simulated cell voltage (filled circle) of the detailed center cell and the average voltage of experiment and simulations (vertical dashed lines).

is necessary. The final operation point is in isothermal co-electrolysis operation.

The large temperature differences between the individual locations are striking. In exothermic operation points, in both SOFC and SOEC mode, the difference can exceed 100 K. By operating the reactor around the isothermal point, the differences can be minimized. Due to the endothermal reverse water-gas shift reaction, the differences are smaller in co-electrolysis mode than in water electrolysis. For the exothermic operation points, the spatial temperature difference across the cells is significantly smaller than the reactor inlet and cell outlet. It follows that, a reactor inlet temperature that is 200 K lower than the cell outlet temperature, can result in a cell temperature difference of only 100 K due to the internal preheating in the reactor. The temporal temperature gradients depend mostly on the ramp speeds and the quality of the temperature controller. Decreasing the spatial and temporal gradients for specific systems will be done in the future using the simulation framework.

Operation of SOC reactors with local degradation.—As the validation study showed, an important aspect to be considered in SOC reactors is the non-uniform degradation of individual stacks. Degradation and an operation strategy for unevenly degraded SOC reactors will be investigated by increasing the degradation factor presented above. An extreme case is the fast degradation of one single stack, which is considered here. It was analyzed for co-electrolysis operation with the SOC reactor shown above. The inlet fuel flow, with the molar composition 10% H_2, 57% H_2O and 33% CO_2, was calculated to achieve a reactant conversion of 70% at -0.55 A cm^{-2}. The air flow on the oxygen side was set to 11 g s^{-1}. Both, the fuel and air inlet temperature were set to 830 °C.

Figure 12 shows the temperatures profiles of all towers while only stack T1S3 degrades over time. As the control system did not react, stack temperature and voltage increased. The surrounding stacks were also affected due to heat transfer. In the fourth timestep, temperature and voltage were rather high and the operation should have been stopped to avoid further damage.

An operating strategy that allows the operation of this reactor, is monitoring the individual stack voltages and controlling the electric currents to maintain a maximum voltage (here 1.4 V). When the maximum voltage is exceeded, the electrical current will be reduced using a proportional gain. This option allows the reactor to continue operating at reduced power. In the case of this specific reactor, the electrical currents of individual towers can be controlled separately. Thus, only the current of tower 1 is reduced.

This results in a reduction of the temperatures of the stacks connected in series. The other electrical channels will continue to operate at the initially set current. Therefore, the reactant conversion and thus the product gas composition will be different. This can be seen from the change in the reactant conversions ΔRC of the individual stacks. In the constant current case (Fig. 12), the conversion of the single stacks changes slightly due to an increased pressure loss ($\Delta p = f(\rho) = f(T)$) in the degraded stack. In case of co-electrolysis this will lead to a slight change in the product gas composition depending on the water-gas shift equilibrium. In case the voltage is limited (Fig. 13), the conversion of the stack tower that exhibits the decreased electrical current will drop. This will lead to a stronger change in the product gas composition. To avoid this,

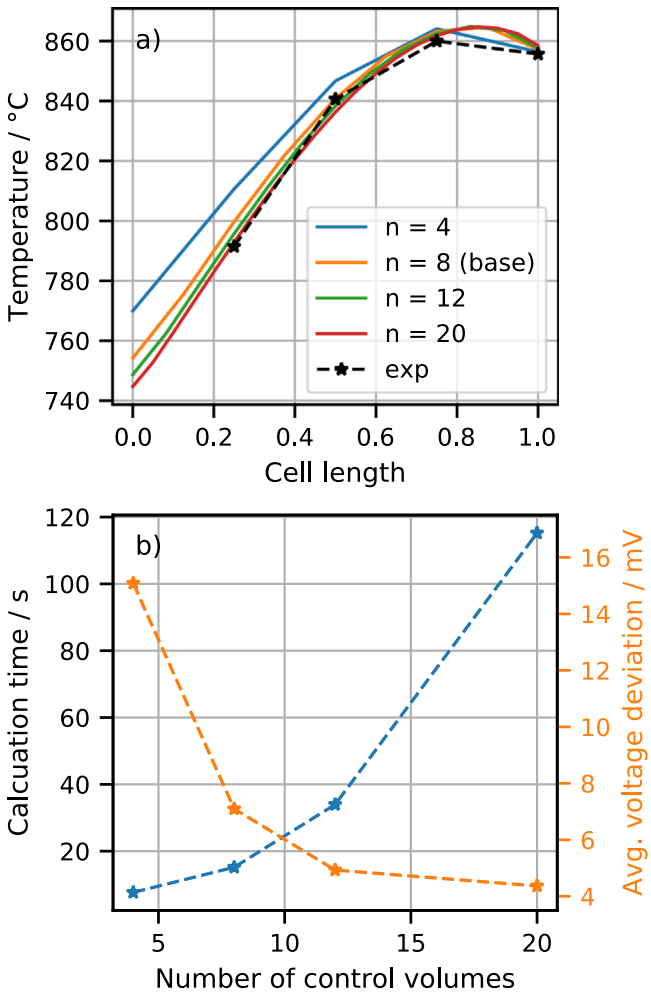

Figure 8. Variation of number of control units for one representative operating point. The simulation results show the values for the center cell of the stack. The part (b) of the figure shows the dependency of calculation time and voltage deviation.

smaller clusters could be formed, which can be electrically controlled independently of each other. However, this increases complexity and costs.

A third option that lies between the two discussed scenarios, is the parallel connection of the towers. In that case, the control system would not react but the electrical current of the first tower would decrease, due to the higher electrical resistance. The current of towers 2 and 3 would therefore increase. As in the case that is shown in Fig. 12, the operation must be stopped when voltage and temperatures increase above their limits. Additionally, temperature, voltage, and reactant conversion of towers 2 and 3 must be monitored.

SOC reactor scaling.—For SOC reactors to play a role in the energy system of the future, the power rating must be increased. In addition to increasing the cell area, there are two options for accomplishing this: the number of stacks per SOC reactor or the number of SOC reactors can be increased. By increasing the number of stacks, thermal losses can be minimized but flow distribution becomes more challenging. In this work the number of stacks will be increased by increasing the height of the stack towers. Subsequently, a lumped heat capacity will be derived for system simulations with a simpler model. The simulation of plants with several SOC reactors will be extensively investigated in a future work.

Increase of tower height.—The capacity of an SOC reactor can be increased, for example, by a higher number of stacks per stack tower. This is examined in Fig. 14 for isothermal and exothermal electrolysis operating points. The inlet fuel flow with the molar composition 10% H_2 and 90% H_2O is calculated to achieve a reactant conversion of 70%. In isothermal operation the air flow on the oxygen side is calculated to achieve an oxygen output composition of 50%. Both the fuel and air inlet temperature are set to 830 °C. In exothermal operation, the air flow is set by a PI controller to keep the maximum temperature at 855 °C, and the inlet temperatures are set to 750 °C.

The selected operating conditions lead to a wider temperature range in exothermic operation, which increases with an increasing number of stacks. Due to the higher current in exothermic operation, higher cell voltages occur. As the number of stacks increases, the voltage behaves contrary. In exothermic operation, the voltage increases and the efficiency decreases. In isothermal operation, however, the cell voltage decreases and a higher efficiency is achieved. The electric current also decreases, due to decreasing specific heat losses, which in turn causes an increase in efficiency. However, the efficiency increase is greater than expected for the sheer current reduction.

This can be explained by the fact that the reactor surface per stack and thus the heat losses per stack decrease with increasing stack number. As a result, the temperature in isothermal operation increases, while the minimum temperature in exothermal operation decreases. This is due to the fact that in exothermic operation the reactor is cooled by the air flow. Consequently, heat losses must be avoided in isothermal operation, since these reduce efficiency. In contrast, during exothermic operation, heat losses evenly distributed

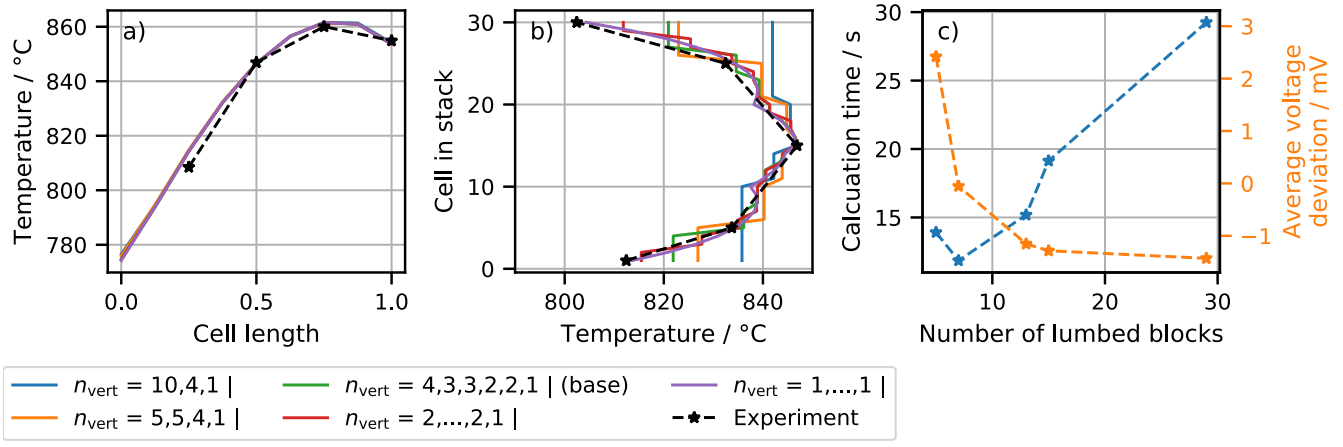

Figure 9. Variation of the vertical simplified block size for one representative operation point. The vertical bar sign indicates the symmetry line. The impact on the center cell was minimal.

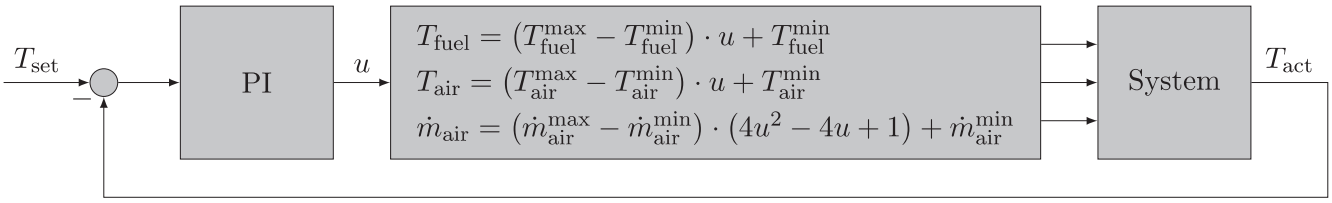

Figure 10. Temperature controller for operation of SOC reactors at various operation points.

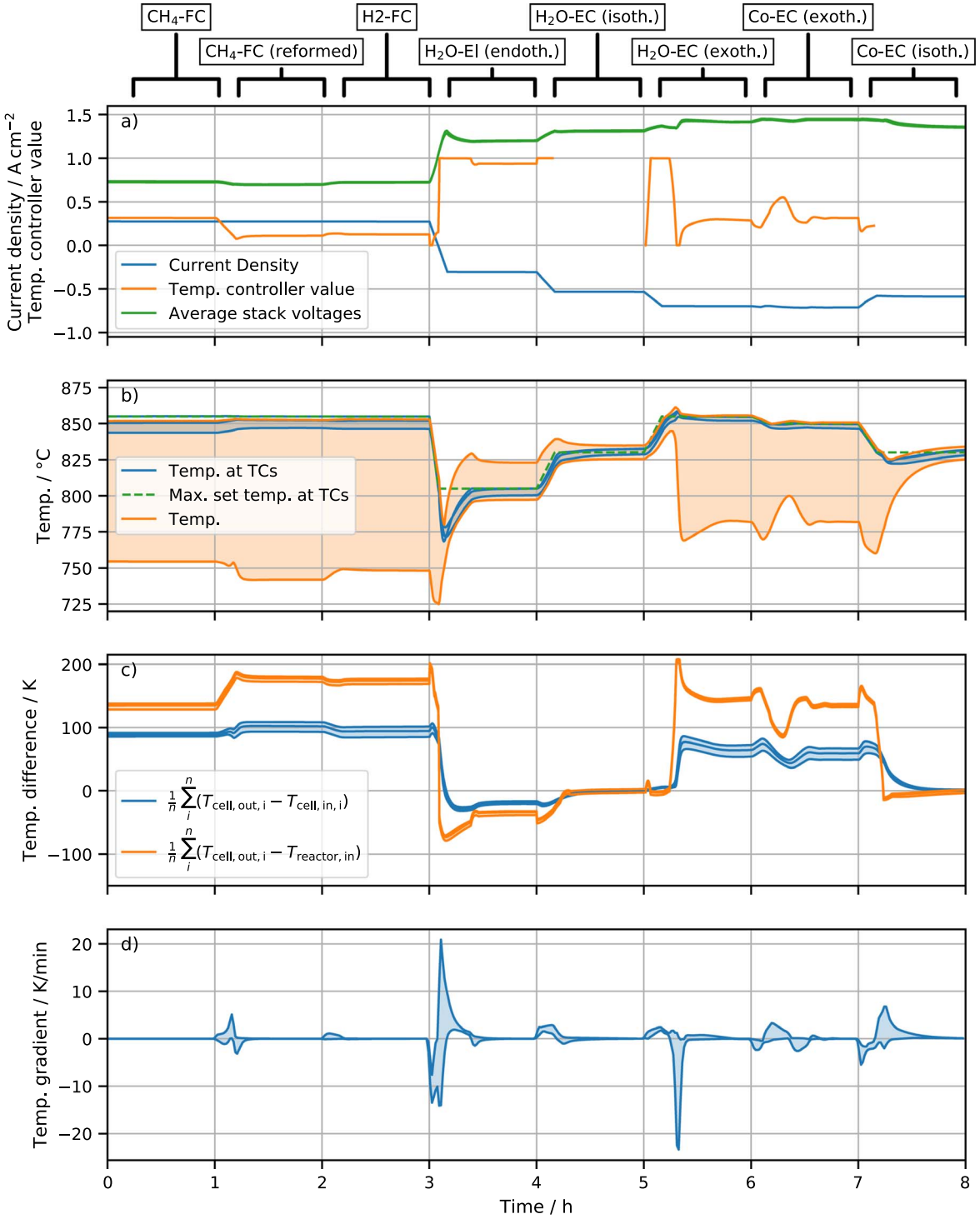

Figure 11. Operation of the SOC reactor in eight different operation points with transient maneuvers using the temperature controller described above.

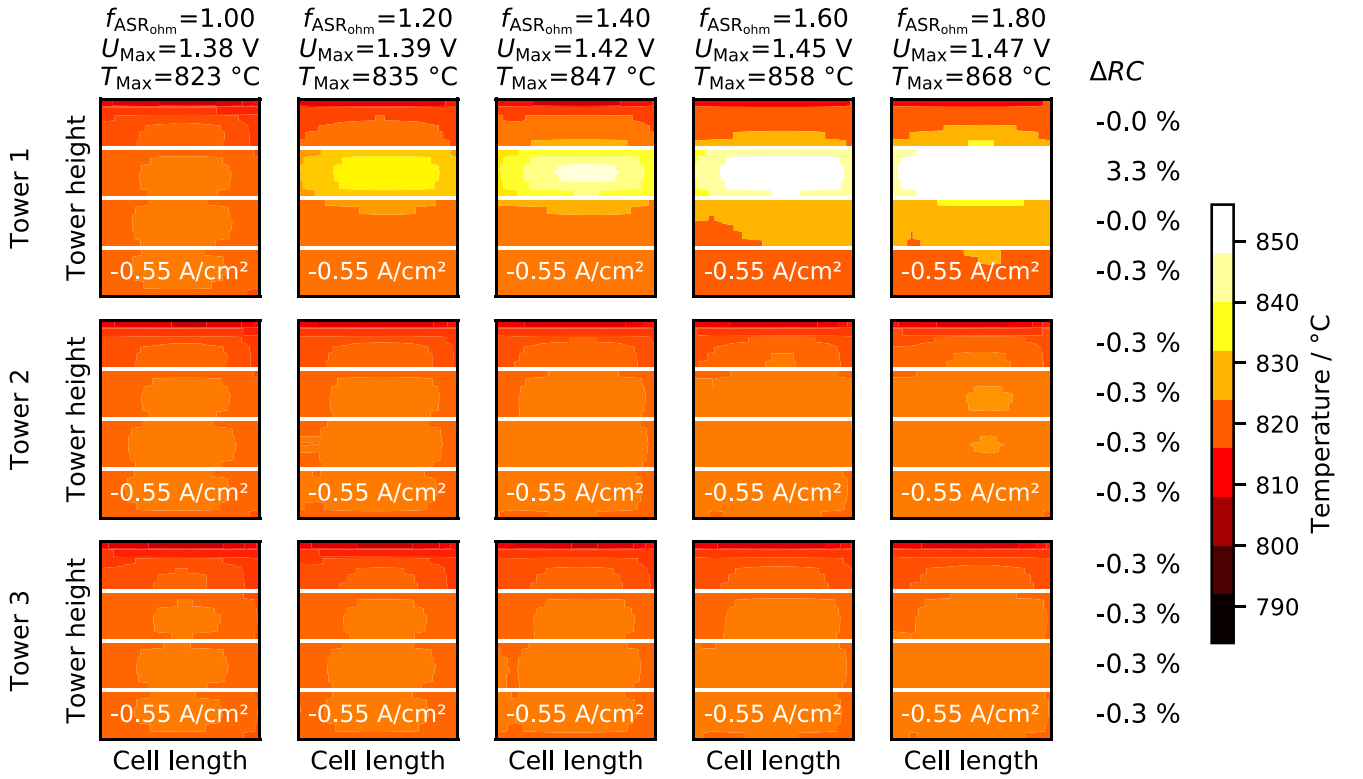

Figure 12. Degradation of stack T1S3 over time. In the first timestep/column, the degradation has not started yet. The temperature profile is even. In the second timestep, the ohmic ASR of stack T1S3 is increased by 20% leading to an increased temperature and a slightly higher voltage. This continues in the further time steps. As the control system does not react, temperature and voltage of stack T1S3 exceed their limit around timestep four. Furthermore, the surrounding stacks are also affected due to heat transfer.

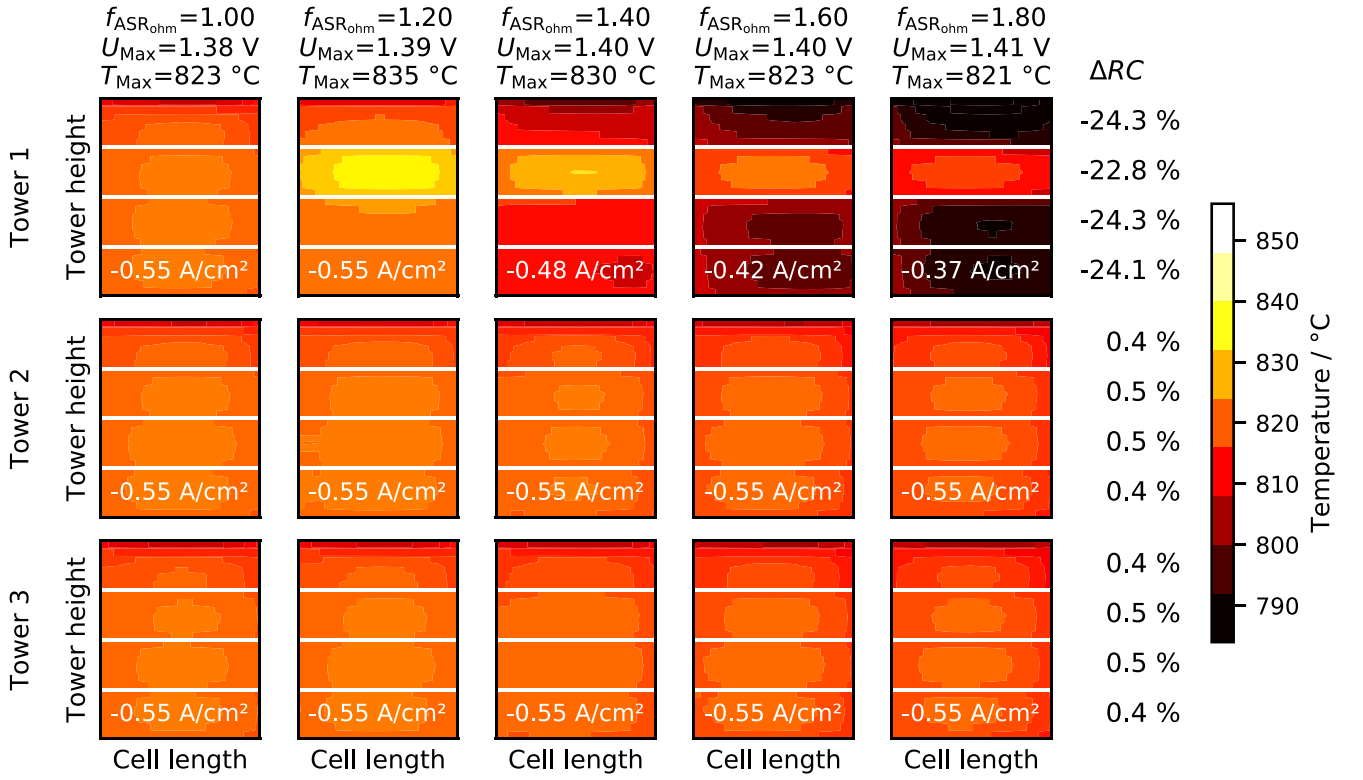

Figure 13. Degradation of stack T1S3 over time. Between timestep 2 and 3 the control system starts to decrease the electrical current of the tower limiting the average cell voltage to 1.4 V. This results in a reduction of the temperatures of the stacks connected in series. The temperature and voltage will not exceed the upper limits. However, the lower temperature limit should be monitored.

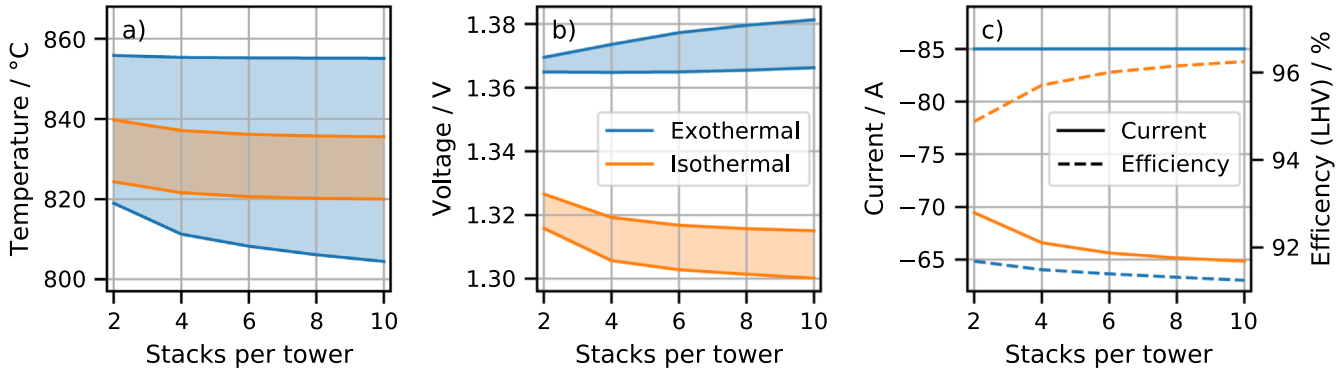

Figure 14. Change in temperature (a), voltage (b), current (c, left ordinate) and efficiency (c, right ordinate) when varying the number of stacks per tower in isothermal and exothermal operation. The areas cover the entire SOC reactor from minimum to maximum value.

over the reactor are helpful, since a lower cooling flow and thus a lower spatial temperature difference is achieved. However, large local heat losses due to thermal bridges should be avoided in any case, since they lead to individual cells and stacks being operated outside the permissible operating range.

Calculation of a lumped heat capacity.—By simulating transitions, a lumped heat capacity C_{Reactor} can be calculated for the described reactor, which can be used as a basis for further system modeling with simpler models. Since the ratio of the heat capacity of the cells to the heat capacity of the other components changes when the reactor is scaled, the lumped heat capacity is given here as a function of the power.

$$\frac{C_{\text{Reactor}}}{P_{\text{el,DC,nominal}}} = a_i \left(\frac{P_{\text{el,DC,nominal}}}{1\ \text{kW}} \right)^{-\frac{-6.00 \cdot 10^{-5}}{\text{K}} T - 0.0596}$$

$$\text{with } a_{\text{FC}} = \left(\frac{0.0101}{\text{K}} T + 18.2 \right) \frac{\text{kJ}}{\text{kW K}} \text{and}$$

$$a_{\text{EC}} = \left(\frac{0.00623}{\text{K}} T + 16.9 \right) \frac{\text{kJ}}{\text{kW K}}$$

The interpolation was done with simulation data from 300 °C to 800 °C and reactors from 30 kW/6 kW to 235 kW/43 kW in electrolysis and fuel cell mode, respectively.

Summary of the analysis of SOC reactors with multiple stacks.—Figure 15 summarizes the impacts of heat losses and pressure losses on an SOC reactor with multiple stacks, for isothermal and exothermal electrolysis operation, derived from the presented and additional simulations results. It shows which parameters are affected, and in which cases, limits can be exceeded, leading to illegitimate operation points. The conclusions for exothermal electrolysis operation can also be applied to fuel cell mode. Scaling of SOC reactors with multiple stacks, leads to lower heat losses per stack (assumed as uniform), as the reactor surface per stack will decrease. However, due to longer pipes and more complex manifolds, the pressure losses could increase.

In case of heat losses, it must be distinguished between uniform and local losses. Uniform losses affect all stacks in the reactor, while local losses only affect a single stack. Both, uniform and local are theoretical extreme cases, that help to understand the impact of heat losses. In reality, heat losses are always a combination of these extremes. In case the heat losses per stack increase uniformly, the temperatures of all stacks decrease. If an isothermal operation is wanted, the electrical current needs to be increased. This increases cell voltage and decreases efficiency. In exothermal operation, an increasing uniform heat loss decreases the necessary cooling power, leading to a lower spatial temperature difference and a higher efficiency. However, this efficiency will be still lower compared to the isothermal operation. In case of increasing local heat losses, the temperature of single stacks will decrease, resulting in a lower efficiency or even too high voltages.

Increasing pressure losses lead to an uneven flow distribution on fuel and oxygen side. On the fuel side, this can lead to locally high reactant conversions and thus high voltages, which could exceed their limits. Due to the low air flow needed in isothermal operation, the maximum oxygen content could be exceeded locally. Furthermore, in exothermal operation, the cooling air flow in the individual stacks varies, which could lead to temperature limits being exceeded.

Conclusion and Outlook

In this work, a transient modeling framework for the investigation of an SOC reactor with multiple stacks was developed. The novelty of the used approach, is the representation of all cells and stacks in the reactor. For this purpose, the modeling of the individual subcomponents, in particular the stack, was explained. Using a simplification approach for the stack model, which limits the calculation of chemical and electrochemical processes to a few cells by distribution of the relevant information, the overall calculation time was reduced by an order of magnitude resulting in fast and reliable stack simulations. By modeling pipes, manifolds and insulation, important effects such as heat and pressure losses were represented. It could be shown that the simulation results reproduce measured values well and the model was experimentally validated.

The simulation results show that models of SOC reactors with multiple stacks are necessary to analyze heat losses and flow distribution leading to non-uniform temperature and voltage distributions over the stacks of SOC reactors. Thus, individual cells and stacks can exceed their operating range, which lead to lower performance and higher degradation. The detection of these exceedances is not always possible by experimental means, as commercial SOC reactor have only a limited number of sensors, or by usage of simple simulation models. This work demonstrated that the missing information can be obtained from simulations with this framework. As a consequence, the operation can be made more performant and reliable.

For example, a simulation study over a wide operating range showed that the temperature difference between locations equipped with thermocouples and the overall reactor can surpass 100 K in exothermal operating points. This is primarily due to the temperature difference over the flow length of the cells, at lower inlet temperatures. But also differences over the tower height lead, for example, to low temperatures and thus high overpotentials at the upper and lower cells.

The study shows that the two main challenges, how to operate SOC reactors with multiple stacks, and how to scale them; can be addressed with the TEMPEST framework developed in this work.

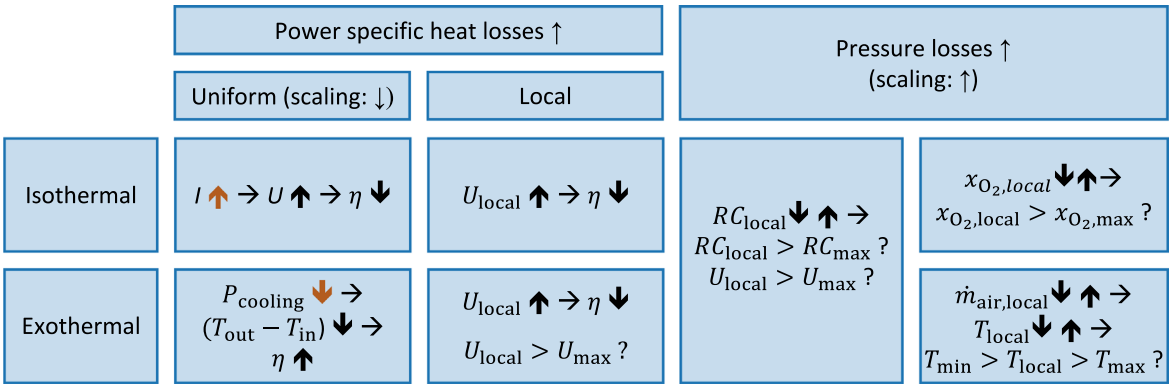

Figure 15. Summary of the impact of heat losses and pressure losses on an SOC reactor with multiple stacks. The up and down arrow indicate an increase or decrease of the value, question marks symbolize the risk of exceeding a limit and "local" means that only certain stacks are affected. Orange arrows specify reactions of a control system. Uniform losses affect all stacks in the reactor while local losses only affect a single stack.

Therefore, the model will be used in further research to investigate and enhance the operation of specific systems, like a power-to-chemicals plant with CO_2 air capture, by developing operation and control strategies. In addition, the simulation framework will be applied to other electrochemical technologies such as SOC reactors with electrode supported cells and even alkaline electrolysis systems.

Acknowledgments

This work was financially supported by the Federal Ministry of Economic Affairs and Energy under grant number 03EIV031C. The responsibility for the contents lies with the authors. The authors would like to thank Sunfire GmbH for providing the experimental stack results and the parameters. Furthermore, the authors express their gratitude to the entire TEMPEST team for their work on the simulation framework.

ORCID

M. Tomberg https://orcid.org/0000-0001-7798-4229
M. P. Heddrich https://orcid.org/0000-0002-7037-0870
F. Sedeqi https://orcid.org/0000-0003-2883-6494
D. Ullmer https://orcid.org/0000-0002-0782-6759
S. A. Ansar https://orcid.org/0000-0001-6300-0313
K. A. Friedrich https://orcid.org/0000-0002-2968-5029

References

1. A. Hauch, S. D. Ebbesen, S. H. Jensen, and M. Mogensen, *J. Mater. Chem.*, **18**, 2331 (2008).
2. S. H. Jensen, X. Sun, S. D. Ebbesen, R. Knibbe, and M. Mogensen, *Int. J. Hydrogen Energy*, **35**, 9544 (2010).
3. A. B. Stambouli and E. Traversa, *Renew. Sustain. Energy Rev.*, **6**, 433 (2002).
4. T. A. Adams, J. Nease, D. Tucker, and P. I. Barton, *Ind. Eng. Chem. Res.*, **52**, 3089 (2012).
5. M. Navasa, X.-Y. Miao, and H. L. Frandsen, *Int. J. Hydrogen Energy*, **44**, 23330 (2019).
6. R. Peters, M. Frank, W. Tiedemann, I. Hoven, R. Deja, N. Kruse, Q. Fang, L. Blum, and R. Peters, *J. Electrochem. Soc.*, **168**, 014508 (2021).
7. S. Santhanam, M. P. Heddrich, M. Riedel, and K. A. Friedrich, *Energy*, **141**, 202 (2017).
8. C. Geipel et al., *ECS Trans.*, **91**, 123 (2019).
9. M. C. Williams, S. D. Vora, and G. Jesionowski, *ECS Trans.*, **96**, 1 (2020).
10. M. Tomberg, M. Metten, C. Schnegelberger, M. P. Heddrich, A. Ansar, and K. A. Friedrich, *14th European SOFC & SOE Forum 2020* (Zenodo, Lucerne) (2020).
11. M. Tomberg, S. Santhanam, M. P. Heddrich, A. Ansar, and K. A. Friedrich, *ECS Trans.*, **91**, 2089 (2019).
12. M. Tomberg, M. P. Heddrich, M. Metten, S. A. Ansar, and K. A. Friedrich, *Energy Technology*, **10**, 2101075 (2022).
13. S. Srikanth, M. P. Heddrich, S. Gupta, and K. A. Friedrich, *Appl Energ*, **232**, 473 (2018).
14. M. Li, J. Brouwer, A. D. Rao, and G. S. Samuelsen, *J. Power Sources*, **196**, 5903 (2011).
15. D. Oryshchyn, N. F. Harun, D. Tucker, K. M. Bryden, and L. Shadle, *Appl Energ*, **228**, 1953 (2018).
16. L. Magistri, R. Bozzo, P. Costamagna, and A. F. Massardo, *J. Eng. Gas Turbines Power*, **126**, 516 (2004).
17. E. Achenbach, *J. Power Sources*, **49**, 333 (1994).
18. V. Menon, V. M. Janardhanan, S. Tischer, and O. Deutschmann, *J. Power Sources*, **214**, 227 (2012).
19. S. Wahl, A. G. Segarra, P. Horstmann, M. Carré, W. G. Bessler, F. Lapicque, and K. A. Friedrich, *J. Power Sources*, **279**, 656 (2015).
20. S. Fogel, H. Kryk, and U. Hampel, *Int. J. Hydrogen Energy*, **44**, 9188 (2019).
21. R. Lin, *1D+1D modeling of reversible Solid Oxide Cell (rSOC) reactors for steady state and dynamic process analyses of electricity storage systems*, Technical University of Berlin / German Aerospace Center (DLR) (2018), https://elib.dlr.de/126289/.
22. F. Sedeqi, "High Temperature Co-Electrolysis Model for Sector Coupling." *Thermodynamic and Detailed Models of Solid Oxide Electrolysis Cells and Systems*, KTH Royal Institute of Technology/German Aerospace Center (DLR) (2020), http://urn.kb.se/resolve?urn=urn:nbn:se:kth:diva-286048.
23. M. Riedel, M. P. Heddrich, and K. A. Friedrich, *Int. J. Hydrogen Energy*, **44**, 4570 (2019).
24. M. Riedel, M. P. Heddrich, and K. A. Friedrich, *J. Electrochem. Soc.*, **167**, 024504 (2020).
25. L. Bobrova, D. Andreev, E. Ivanov, N. Mezentseva, M. Simonov, L. Makarshin, A. Gribovskii, and V. Sadykov, *Catalysts*, **7**, 310 (2017).
26. E. V. Rebrov, *Advances in Clean Hydrocarbon Fuel Processing*, ed. M. R. Khan (Woodhead Publishing, Oxford) p. 387 (2011).
27. M. Riedel, M. P. Heddrich, A. Ansar, Q. Fang, L. Blum, and K. A. Friedrich, *J. Power Sources*, **475**, 228682 (2020).
28. F. Casella and A. Leva, *Math. Comput. Modell. Dyn. Syst.*, **12**, 19 (2006).
29. F. Casella, (2002), ThermoPower, Politecnico di Milano, https://casella.github.io/ThermoPower/.
30. SILCA, *Service- und Vertriebsgesellschaft für Dämmstoffe mbH* (Mettmann, Germany) p. 26 (2018).
31. O. Posdziech, T. Geißler, K. Schwarze, and R. Blumentritt, *ECS Trans.*, **91**, 2537 (2019).
32. S. Santhanam, D. Ullmer, Z. Wuillemin, E. Varkaraki, C. Beetschen, Y. Antonetti, and A. Ansar, *ECS Trans.*, **91**, 159 (2019).